FACTA UNIVERSITATIS
Series: **Electronics and Energetics** Vol. 34, Nº 3, September 2021, pp. 415-433
https://doi.org/10.2298/FUEE2103415R

Original scientific paper

A HIGH EFFICIENCY PNEUMATIC DRIVE SYSTEM USING VANE-TYPE SEMI-ROTARY ACTUATORS

Alfred Rufer

EPFL Ecole Polytechnique Fédérale de Lausanne, CH1015 Lausanne, Switzerland

Abstract. *A compressed air driven generator is proposed, where the pneumatic energy is converted into mechanical energy using two vane-type rotational actuators. The use of a second actuator with a higher displacement in order to produce a thermodynamic expansion allows to reach a better energetic efficiency in comparison to the classical operation of such actuators. The alternating movement of the angular actuators is transformed into a unidirectional rotational motion with the help of a mechanical motion rectifier. The paper analyses the enhancement of the energetic performance of the system. An experimental set-up is also described. The performance of the new system is described, and the limits of its realization is commented on the base of experimental recordings of the evolution of the pressure in the chambers.*

Key words: *compressed air motor; energy efficiency; adiabatic expansion; compressed air energy storage; pneumatic actuators; motion rectifier*

1. INTRODUCTION

Renewable energy sources have been developed principally during the last decades of the 20th century and got their technical and economical maturity in the early years of the 21st. These developments are however accompanied by new questions and aspects of availability and intermittency like weather, day and seasonal cycles. These conditions are the main motivations for the development of energy storage techniques.

Near the classical storage technologies with the example of pumped hydro plants, battery energy storage facilities seem to be well adapted solutions for the decentralized energy production. Recent developments of the advanced Li-ion batteries and of their production facilities have led to the actual situation of their high performances in energy and power density, together with their economic aspects [1].

Received December 11, 2020; received in revised form March 3, 2021
Corresponding author: Alfred Rufer
EPFL Ecole Polytechnique Fédérale de Lausanne, CH1015 Lausanne, Switzerland
E-mail: alfred.rufer@epfl.ch

Beneath interrogations about the available material resources for a wide expansion and mass production of batteries for electrical systems as distributed generation or electric mobility, other open questions remain as the possible life cycles and aging effects of electrochemical energy carriers. Finally, the questions about recycling the battery materials are of an actual topic of many researches, looking for answers to technical and economic challenges.

In such a context, many alternative solutions for energy storage are investigated as technologies based on reversible physics like mechanical or thermodynamic principles.

Compressed air energy storage (CAES) belongs to the list of candidate solutions, using only classical materials and established technology. In addition, and in opposition to the electrochemical batteries, these systems can be repaired or refurnished, offering incomparable longer life cycles. Additionally, their materials are not problematic for recycling.

The development of CAES systems includes the development of high-performance compression and expansion machinery and must be in accordance with the elementary rules of thermodynamics. By many different development projects, focus has been set on the isothermal compression and expansion [2], [3], [4] in order to reach the best possible efficiency. Also elementary conversion based on classical pneumatic equipment have been proposed, where the operating principle has led to scarce performance.

In this paper, a new solution is analysed for the energy conversion from compressed air to mechanical and electrical power. The proposed system is based on the use of vane-type rotary actuators, from which the oscillating movement of the rotor is transformed into a unidirectional rotational motion using a so-called motion rectifier to drive the electrical generator [5], [6], [7], [8].

The paper describes the enhancement of the energy efficiency of the pneumatic to mechanical transformation, where in addition to the classical displacement work of the actuator an expansion volume is added to the system allowing to recover an important part of the primarily injected enthalpy [9].

First the operation principle of the original system is presented, which is an electric generator driven by one actuator only and driven under constant pressure as all common pneumatic devices (Fig. 1a). The typical variables as the pressure or the developed torque are simulated, and the resulting energetic efficiency is evaluated.

Then, the modified system with enhanced efficiency is presented where an expansion volume is added which allows to exploit the internal energy of the pressurized air (Fig. 1b). The performances and typical variables are evaluated by simulation.

Finally, a third system is studied in which the same energetic performance as for the previous system can be achieved with one actuator only, where the displacement work and the expansion of the air are executed inside of the same chambers by a dedicated control of the intake and exhaust valves (Fig. 1c).

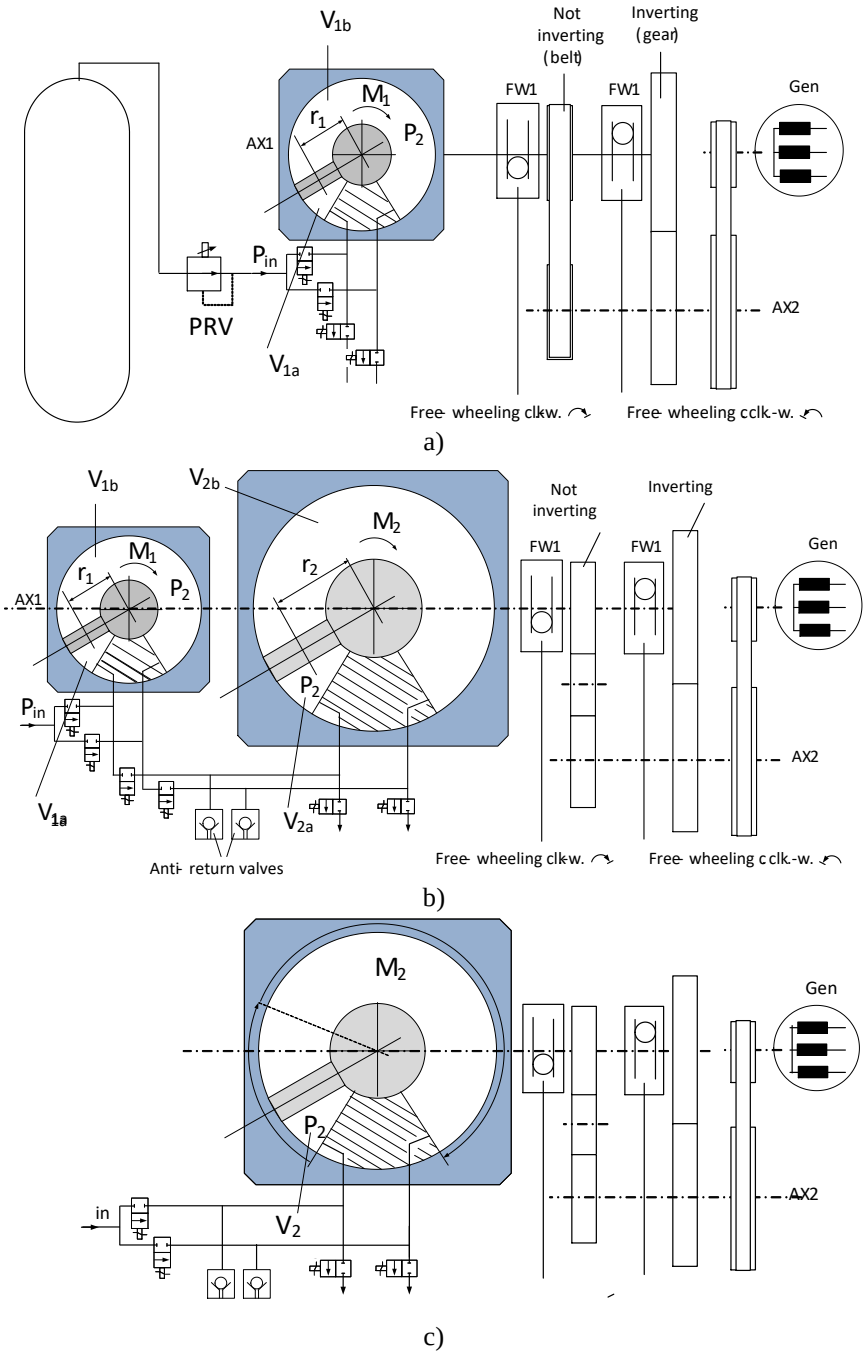

Fig. 1 The three versions of the compressed air driven generator a) the original system, b) the system with enhanced efficiency, c) the simplified system with the same enhanced efficiency

2. Torque and Mechanical Work Produced by the Three Systems

2.1. The basic concept of the air-powered diver lamp

Gianfranco Gallino, a genius inventor from southern Switzerland has realized and patented an original lamp for divers, using as energy reservoir the same air bottle as for the breathing air. The conversion of the energy from its pneumatic form into electric power for the lighting bulb is realized by a pneumatic vane-type semi-rotary actuator driving an electric generator. Figure 1a) shows the patented system of Gallino with its main parts as the high-pressure air bottle, the pneumatic actuator with the motion rectifier and the electric generator for the powering of the bulb.

At the left side of Fig. 1a), the air reservoir is connected to a pressure reduction and regulation valve (PRV), which reduces the air pressure from the reservoir to the operation pressure of the vane type angular actuator. This actuator comprises two working chambers, fed alternatively by pressurized air through the control valves. The motion rectifier is composed of two driving trains, the first being of the direct non-inverting type, realized with a toothed belt. The second train is an inverting gear. Both trains are driven from the input shaft in their respective direction through two free-wheeling devices working in the clockwise and counter-clockwise directions, resulting in a unidirectionally rotating output shaft. This output shaft is connected to the electric generator through a simple multiplying gear in order to reach a sufficiently fast speed of the generator.

2.1.1. The typical curves characterizing the Gallino system

The pneumatic actuator of the Gallino system has two chambers fed alternatively by the air under pressure. The volumes of the chambers vary linearly with the angular position of the vane rotor. In the chosen example, the 270° excursion of the rotor lasts over 0.5 s for the clockwise and counter-clockwise motion, leading to a period of 1s. The complementary evolution of both chambers is represented in Fig. 2. The maximal value of the volume is equal to 118 cm^3.

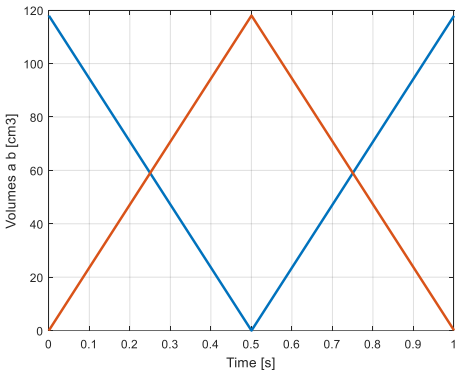

Actuator type	CRB1-63
Volume of chambers	118 cm^3
Torque (10bar)	22 Nm
Radius r	r_1=0.025 m
Surface of wing	S_1=10 cm^2

Fig. 2 Evolution of the volumes of the chambers of the rotary actuator

The actuator is fed by air at a pressure of 10 bar, generating torque contributions on the two sides of the vane. Fig. 3 shows a simple model simulation of the two torque components, composed of the action of the feeding pressure during the first respectively the second half period, and the action of the atmospheric pressure during the second

(respectively the first) half period when the exhauxt valves are open. In this simulation, the dynamic response of the air-flow into the chambers is not considered, but in reality, the tubing section and length as the size of the control valves will have an influence as was recognized in the experimental set-up (see section 5).

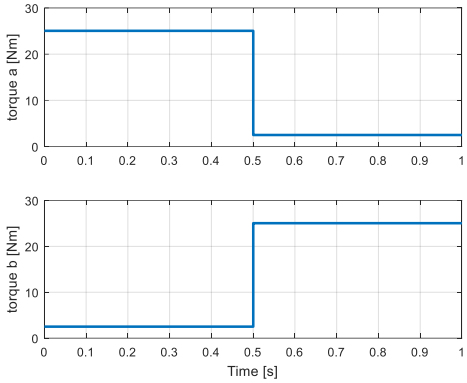

Fig. 3 Torque contributions of the left and right sides of the rotor vane

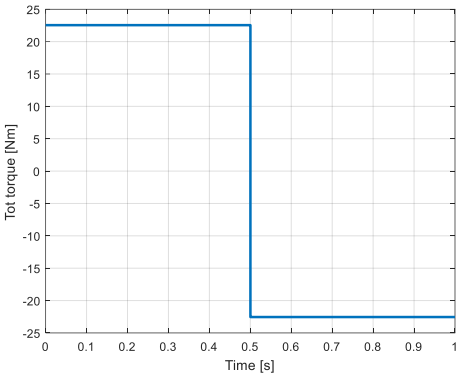

Fig. 4 Resultant torque of the actuator

The evolution of the resulting torque of the actuator according the simple model is represented in Fig. 4 and shows the alternance of its sign depending on the rotor's motion. In this simulation, the rotor's inertia is neglected, and the reversal of the motion is supposed to be infinitively short. The real motion of the rotor will be considered in the simulation of the third system in section 4.

At the output side of the motion rectifier, the torque is applied to the generator in one direction only. The "rectified" torque of the first system (Gallino) is represented in Fig. 5.

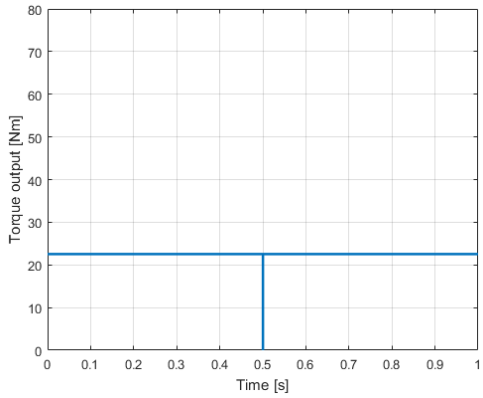

Fig. 5 Torque at the output side of the motion rectifier

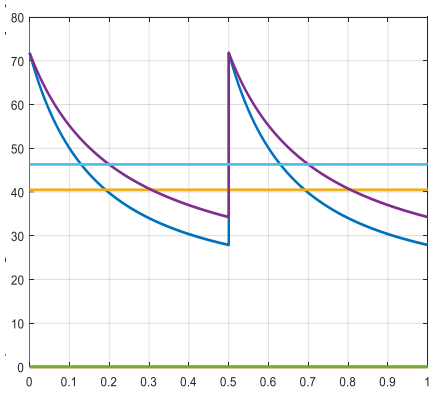

Fig. 6 Torque developed with the system with an additional expansion volume. The figure shows adiabatic (blue and yellow) and isothermal (violet and light blue) expansions together with their averages.

Fig. 6 anticipates for comparison the result of the simulation of the second system with an additional expansion device as represented in Fig. 1b). It is clearly visible that the mechanical performance of this second system is nearly doubled in comparison with the first system.

2.2. The benefit of adding an expansion chamber

Instead of simply opening an exhaust valve and releasing the air under pressure to the atmosphere at the end of the stroke, this air can be expanded in a supplementary actuator of the same type but with larger volumetry and running mechanically in parallel to the first one. Such a system is represented in Fig. 1b). The alternating movement of the coupled rotors is transmitted in the same way through the motion rectifier as in the first described system.

The two vane-type rotary actuators have two active chambers each, corresponding to the volumes V_{1a} and V_{1b}, respectively V_{2a} and V_{2b} (Fig. 1b). The chambers V_{1a} and V_{1b} are fed alternatively by the input compressed air, and they produce torque contributions alternatively according the clockwise and anti-clockwise motions.

The chambers V_{2a} and V_{2b} are fed from the exhaust air of the chambers of the first actuator. The volume V_{2a} receives the exhaust air of the V_{1b} chamber during the clockwise motion, and the volume V_{2b} that-one of the V_{1a} chamber during the anti-clockwise one. Because of the different volumes of the chambers of the first and second actuator, the air-transfer from the chambers of the first actuator to that-ones of the second-one corresponds to a real expansion of the transferred air, allowing so to recover a significant part of the internal energy of the pressurized fluid. In the studied example, the volume ratio of the two actuators is chosen as $V_2/V_1 = 3$.

The evolution of the volumes of the chambers of the actuators is indicated in Fig. 7a and 7b. Fig. 7a shows the volumes of the two complementary chambers V_{1a} and V_{2b} during the two half-periods (0 to 0.5s clockwise and 0.5 to 1s anti-clockwise). Fig. 7b shows the evolution of the two other chambers (V_{1b} and V_{2a}) for the same cycle. In addition, the yellow curve represents the equivalent expansion volume of the interconnected chambers $V_{1b}+V_{2a}$. During the first half-cycle, this last evolution corresponds to a real expansion, but in the second half-cycle, the volume decrease does not have any significant contribution to the torque, the exhaust valve being open.

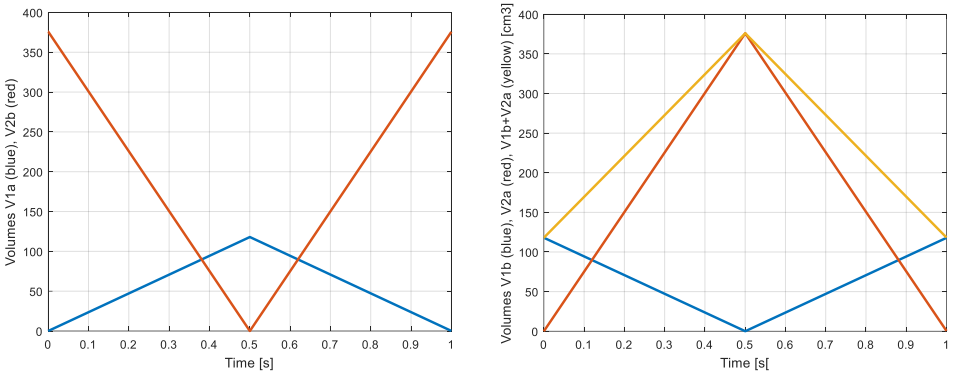

a) b)

Fig. 7 Evolution of the volumes of the two actuators. a) Volumes V_{1a} and V_{2b}, b) Volumes V_{1b}, V_{2a} and $V_{1b}+V_{2a}$

The added actuator is of the type CRB1-100 and has a volume of the chambers equal to 376 cm3. It develops a nominal torque of 75 Nm at 10 bar. Its radius r is 0.038 m, and the surface of the wing is 21cm^2.

2.2.1. The pressure variation during the expansion

The expansion of the air is supposed to be of the adiabatic type, and the resulting pressure P_2 in the chambers V_{2a} (first half-cycle) and V_{2b} (second half-cycle) and of the respective feeding chambers V_{1b} and V_{1a} as-long-as the c-w and a-c-w motions are not completed takes the value of

$$P_2 = P_{in}\left(\frac{V_{1\max}}{V_{1a,b}+V_{2b,a}}\right)^{\gamma} \quad \text{with } \gamma = 1.4 \tag{1}$$

At the end of the two motions, the volume ratio is equal to 1/3, and the corresponding pressure ratio becomes

$$P_{in}/P_2 = 0.21 \text{ according to rel. (1).}$$

In Fig. 8, the pressure P_2 in the expansion volume $V_{1b}+V_{2a}$ is represented (blue curve), together with the pressure in the inlet chamber of the first actuator (P_{in}) (red). While P_{in} is not changing during the motion of the wing, the pressure P_2 is decreasing according rel. (1).

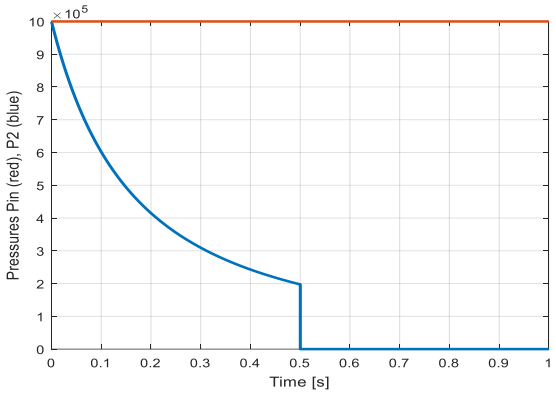

Fig. 8 Pressures P_{in} (red) and P_2 (blue) during the first half of the cycle (clock-wise motion)

If the cascaded actuators are fed from a lower pressure, the expansion can lead to a pressure decrease to a value that is under the atmospheric pressure, producing a negative torque value. In order to avoid this phenomenon, an anti-return valve is connected to the exchange lines between the two actuators [9].

2.2.2. From the pressure to the torque

Figure 9 is representing the evolution of the torque contributions of the first actuator during the first stroke (clock-wise motion) occurring in the first half-period. This torque contributions are related to both sides of the wing. The V_{1a}-side surface S_{1a} is multiplied by the pressure P_{in} to obtain the acting force. Further, this force is multiplied by the corresponding radius r_1 to get the M_{1a} torque component. The effective surface and related radius are given in Table 1. This contribution is represented in red in Fig. 9.

The V_{1b}-side surface S_{1b} is multiplied by the pressure P_2 and further by the same radius r_1 to obtain the M_{1b} torque component (blue curve in Fig.9). M_1 is obtained by subtraction of both components. This torque is represented in yellow in Fig. 9.

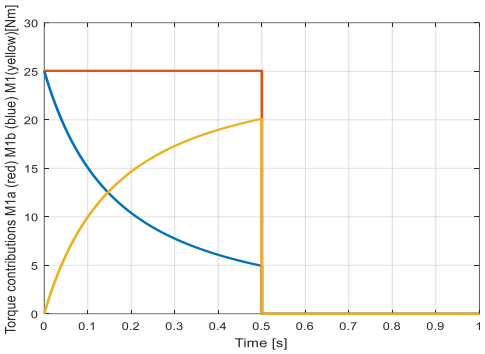

Fig. 9 Torque contributions of the first actuator

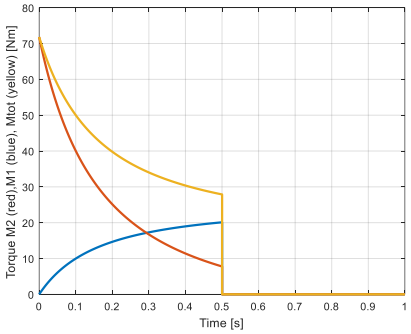

Fig. 10 Torque contributions of the two actuators and total torque during the first half-period

The contribution of the second actuator in the first stroke (clockwise motion) is represented in red in Fig. 10 (M2). This torque results from the V_{2a}-side contribution (effect of P_2, P_2 being the absolute pressure) and the V_{2b}-side where the pressure is equal to the atmospheric pressure. On the same figure, the torque contribution M1 of the first actuator is represented again (blue curve), together with the total torque M_{tot} during the first half-period (yellow curve).

Finally, Fig. 11 shows the total torque during one complete period. The only positive value of the torque indicates that the torque is considered at the output of the motion rectifier. The average value of the torque is also represented. Further, the torque is represented for an expansion occurring in isothermal conditions.

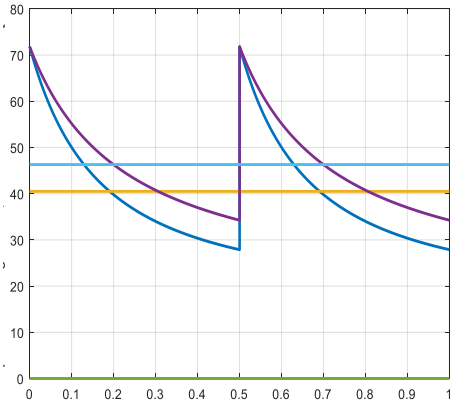

Fig. 11 Torque developed by the two coupled actuators. The figure shows adiabatic (blue and yellow) and isothermal (violet and light blue) expansions together with their averages. X: Time [s], Y: Torques [Nm]

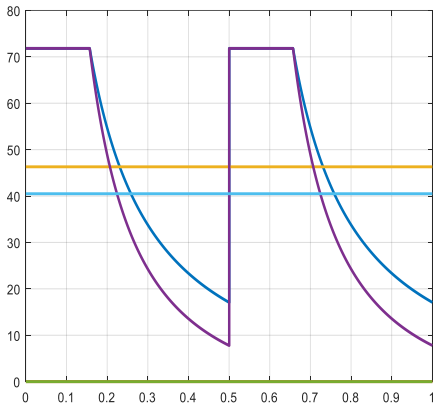

Fig. 12 Torque developed by the large actuator alone (Fig.1c) and with a specific control of the inlet valve. X: Time [s], Y: Torques [Nm]

2.3. Displacement and expansion work in one single actuator

2.3.1. Basic principle

With the third system represented in Fig. 1c) the displacement work and the expansion work are realized in the same device. In the single rotating actuator, the displacement work corresponds to an intake phase under constant pressure, for a volume value comprised between zero and a given volume V1. After this first phase, the intake valve is closed and the air under pressure is expanded while the vane continues its motion up to the end position. The expanded air occupies then the total volume of the chamber V2. To reach the same energetic performance as for the system with two cascaded actuators, the full volume of the single actuator (V2) must have the same value as the volume of the larger actuator of the cascade. The volume V1 of the intake phase is equal to the volume of the small device of the cascade.

For the displacement work at constant pressure and for the expansion work in the same actuator, two rotation angles are defined for one chamber, as for the a-side of the rotating vane, namely the intake angle Φ_int_a, and the expansion angle Φ_exp_a as indicated in Fig. 13. These angles are obtained from the angular sensors shown in Fig. 14.

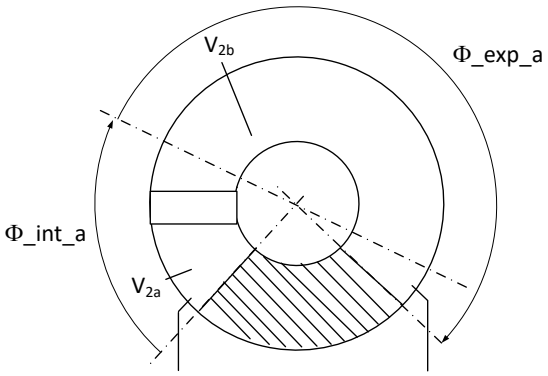

Fig. 13 Intake and expansion angles

The intake phase at constant pressure begins at the origin of the stroke at the a-side of the actuator. Then the intake and the related work at constant pressure lasts over the defined angle Φ_int_a. During this phase, the intake valve at this side (a) is open, the exhaust valve of the opposite side (b) is also open. For the double effect rotary actuator, 4 valves are needed, two for the intakes and two for the exhausts. The principle of adding a non-return valve for each chamber in order to avoid a decrease of the pressure under the atmospheric level remains. The different valves are represented in Fig. 14.

After the intake, an expansion phase lasts for the remaining angle of the stroke Φ_exh_a. During this phase, the intake valve is closed in order to initiate the expansion. The exhaust valve at the opposite side is kept open up to the end of the stroke.

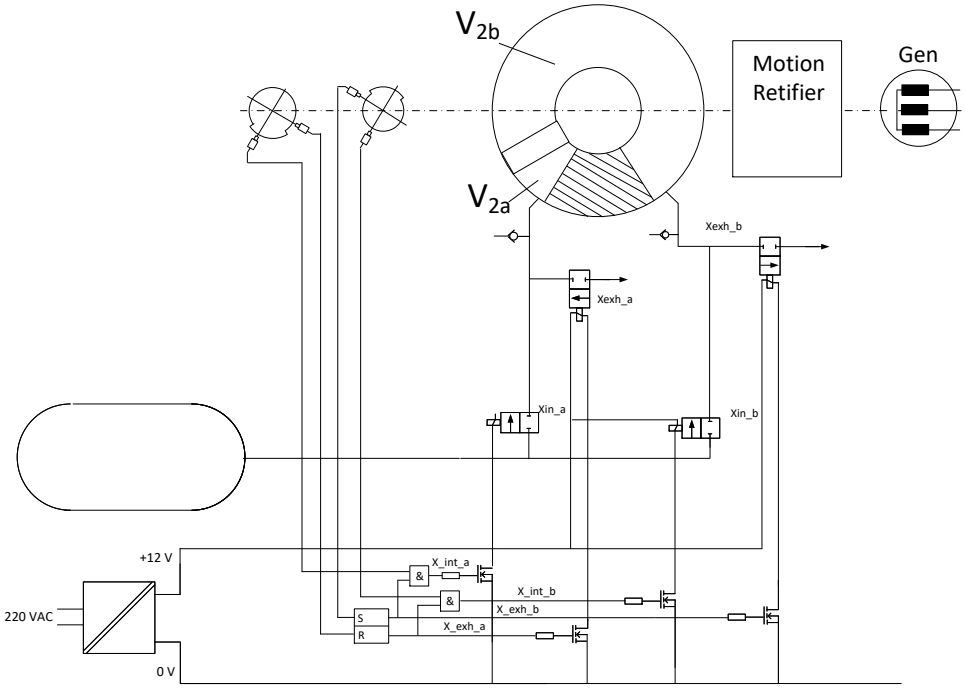

Fig. 14 The complete system of one rotary actuator with displacement and expansion work in the same device

The torque developed by the actuator is composed of two different segments, namely a first constant torque segment corresponding to the intake at constant pressure, followed by a second segment where the torque decreases proportionally to the pressure during the expansion angle. The torque curves are given in Fig. 12. Two different expansion conditions are represented, namely an adiabatic expansion and an isothermal expansion.

3. Comparison of the Efficiencies

3.1. Basics

In a classical pneumatic actuator like a cylinder or an angular actuator, the mechanical work is obtained from the displacement of the piston or the vane under constant pressure P_2 through a volume ΔV (W2, red in Fig. 15). P_2 is generally maintained constant by a pressure release valve. At the end of the stroke, the pressure in the fully deployed cylinder is released to the atmosphere by opening the exhaust valve, allowing the free return of the piston. This corresponds to renounce to the pneumatic energy content inside the cylinder. The pneumatic energy content of the deployed cylinder can be illustrated by the W_{2d} surface (green, right side of V_2) in the diagram of Fig. 15. The maximal value of this energy is obtained under isothermal conditions of the expansion and can be calculated through rel. 2:

$$W_{2d} = P_2 \cdot V_2 \left(\ln \frac{P_2}{P_a} - 1 + \frac{P_a}{P_2} \right) \tag{2}$$

This value will be considered as the internal energy U of the injected air for the calculation of the efficiency in the next paragraph.

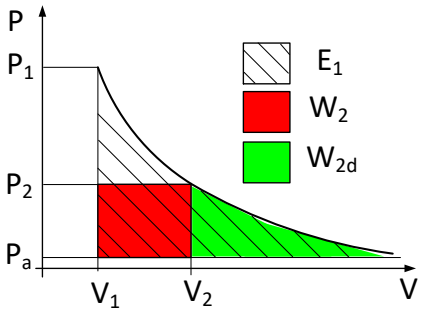

Fig. 15 PV diagram of the air in an actuator

3.2. The efficiency of the single actuator system

The efficiency of the pneumatic motor with a single actuator is calculated on the base of the produced mechanical work and the injected enthalpy into the system:

$$\eta_{conv} = \frac{W_{out}}{H_{in}} = \frac{W_{out}}{U + P_{in} \cdot \Delta V} \tag{3}$$

U is the thermodynamic content of the injected air under pressure and is calculated according rel. (1). Numerically, and considering the two half-cycles, *U* becomes

$$U = E_{comp} = 10 \cdot 10^5 N/m^2 \cdot 2 \cdot 0.000118 m^3 \left(\ln \frac{10bar}{1bar} - 1 + \frac{1bar}{10bar} \right) = 331J \tag{4}$$

$$P_{in} \cdot \Delta V = 10 \cdot 10^5 N/m^2 \cdot 0.000236 m^3 = 236J$$

In this single actuator, the torque produced corresponds to

$$M_1 = M_{1th} - M_{1atm} = 25.05Nm - 2.4Nm = 22.65Nm \tag{5}$$

Then, the angular velocity of the rectified motion is calculated. During the 1 second period of the pneumatic motor, an angle of 270° is run in both directions. After the motion rectification, the output angle is equal to

$$\varphi_{out} = 2 \cdot \varphi_{actuator} = 2 \cdot 270° = 540° \tag{6}$$

The resulting angular velocity becomes

$$\omega_{out} = 2 \cdot \pi \frac{540}{360} \frac{1}{1s} = 2 \cdot \pi \cdot 1.5 rad/s = 9.42 rad/s \tag{7}$$

The corresponding efficiency becomes

$$\eta_{conv} = \frac{W_{out\_single}}{H_{in}} = \frac{M_1 \cdot \varphi_{out}}{U + P_{in} \cdot \Delta V} = \frac{22.65Nm \cdot 9.42rad}{331J + 236J} = 0.376$$

3.3. The efficiency of the motor with two cascaded actuators

For the evaluation of the efficiency of the system with two cascaded actuators, the average value of the developed torque is considered. From the simulation, and as represented in Fig. 11, the average torque value is equal to 40.5 Nm.

The pressure and the intaken volume of air by this system are identic to the previous one. This means that the input enthalpy is identical.

Consequently, and taking into account that the angular velocity is the same, the efficiency becomes

$$\eta_{conv} = \frac{W_{out\_single}}{H_{in}} = \frac{M_1 \cdot \varphi_{out}}{U + P_{in} \cdot \Delta V} = \frac{40.5Nm \cdot 9.42rad}{331J + 236J} = 0.672$$

for an adiabatic expansion.

Under isothermal expansion conditions, the average torque is equal to 46.3 Nm (Fig. 11). The efficiency becomes here

$$\eta_{conv} = \frac{W_{out\_single}}{H_{in}} = \frac{M_1 \cdot \varphi_{out}}{U + P_{in} \cdot \Delta V} = \frac{46.3Nm \cdot 9.42rad}{331J + 236J} = 0.769$$

3.4. Considering the friction in the actuators

To get a more realistic value of the conversion efficiency, the friction torque of the pneumatic actuators must be introduced. The identification of the friction torque has been described in [10]. According to these results, the value of the Coulomb friction torque alone is considered. For a general case, the friction torque is supposed to be equal to 10% of the rated torque of the actuator.

For the single actuator, the effective torque is given by

$$M_{1e} = M_1 - M_{1\,fric} = 0.9 \cdot 22.65Nm = 20.38Nm \tag{8}$$

Then, taking in account of the friction the efficiency becomes

$$\eta_{conv} = \frac{W_{out\_single\_eff}}{H_{in}} = \frac{M_{1e} \cdot \varphi_{out}}{U + P_{in} \cdot \Delta V} = \frac{20.38Nm \cdot 9.42rad}{331J + 236J} = 0.338 \tag{9}$$

For the cascaded actuators, the effective torque is equal to the average torque minus the friction of both individual actuators

$$M_{tot_e} = M_{tot_{av}} - M_{fric\_1} - M_{fric\_2} = 40.5Nm - 0.1 \cdot 22Nm - 0.1 \cdot 75Nm = 30.8Nm \tag{10}$$

The efficiency becomes for the 1s cycle

$$\eta_{conv} = \frac{W_{out\_cascaded}}{H_{in}} = \frac{M_{tot} \cdot \varphi_{out}}{U + P_{in} \cdot \Delta V} = \frac{30.8Nm \cdot 9.42rad}{331J + 236J} = 0.51$$

4. Simulating the System with Sensors and Closed Loop Control

The simulation of the system represented in Fig. 1c) with sensors, control signals and the closed loop operation will consider the real operation of the motion rectifier described at paragraph 2.1. For this purpose, the mechanical model given in Fig. 16 will be used. In this model, a first integration block is representing the movement of the wing-rotor of the actuator alone. At its input side, a factor K1 is used to characterize the inertia of this rotor, K1 being the inverse of the mechanical time constant T_m of the rotor. The action of the motion rectifier corresponds to limit the speed of the rotor to the value of the rotational speed of the output shaft. This value is set as a constant (Omega) in order to simplify the simulation. This parameter could be simulated separately as another mechanical integrator as represented with dotted line in the lower left side of the figure. This additional integrator would simulate the dynamics of the whole output shaft including the electric generator. The limitation function is given through a simple limiting block where the upper limit (Omega) and the lower one (-Omega) are directly imposed. As a result, the speed of the rotor appears at the output of the limiting block.

In reality the angular velocity of the rotor cannot overtake that of the output shaft (Omega), and the output of the first integrator must be controlled with an anti-reset wind-up circuit. This circuit comprises a subtraction block which compares the output and the input of the limitation block. The output of the comparator is fed back to the input with a factor K2.

This factor (100 in this case) controls the static error between the simulated rotor speed and the speed of the output shaft.

Then, the position of the rotor is simulated with a second integrator. The output quantity corresponds to the rotor position.

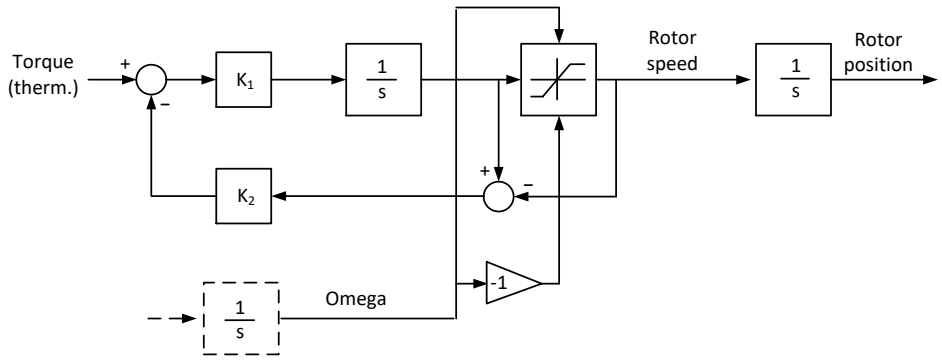

Fig. 16 Mechanical model of the rotor and motion rectifier

From the position of the rotor, the signals produced by the sensors are generated, as well as the control signals for the valves. The computation of the control signals is realized according the description of Fig. 14. Sensors signals and control signals are represented in Fig. 17.

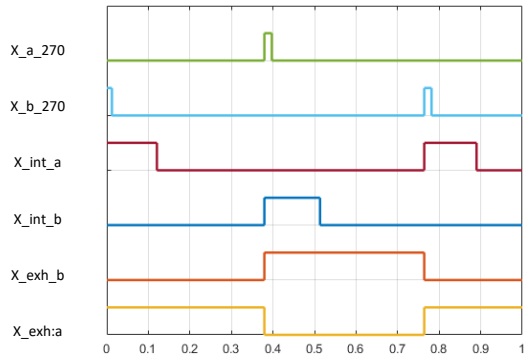

Fig. 17 Signals from the sensors and control signals

In Fig. 18, the speed of the rotor and its position are represented. The angular speed of the rotor is limited through the parameter Omega set to 6.28 rad/s. One can see that the rotor speed jumps from a positive value (Omega) to a negative one (-Omega) with a specific slope, corresponding to the inertia of the wing rotor alone.

The position of the rotor is controlled by the RS flip-flop as represented in Fig. 14 which acts as a kind of two-point controller. The rotation angle swings up and down from nearly zero and 4.71 rad. These values correspond to the end-of-stroke positions of the 270° actuator.

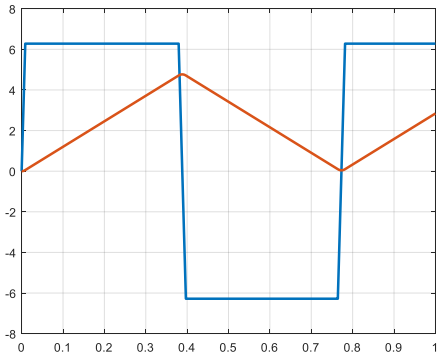

Fig. 18 Rotor speed (blue) [rad/s] and rotor position (red) [rad]

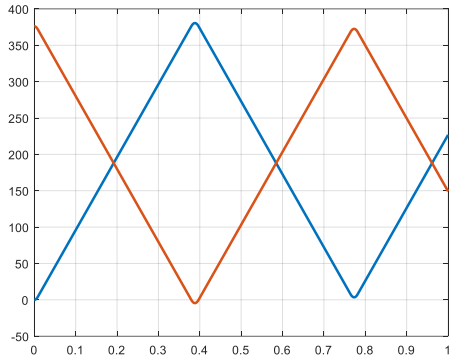

Fig. 19 Volumes of the two chambers of the actuator. Side a (blue) and side b (red) X: Time [s], Y: Volumes [cm3]

From the angular position of the rotor, the volumes of both chambers (a and b) can be easily calculated. They are represented in Fig. 19

Combining the variables representing the volumes and the control signals of the valves, the pressure in each chamber can be calculated. On the curves of Fig. 20, one can clearly distinguish the flat segment at the beginning of the clockwise and anti-clockwise strokes, corresponding to the intake under constant pressure. These segments are followed by the expansion curves when the intake valves are closed.

In the simulation, the expansion is considered in adiabatic conditions. At the end of the expansion, the rotor has reached its end-position and returns in the opposite direction. In this phase, the exhaust valves are open and the atmospheric pressure appears in the chambers.

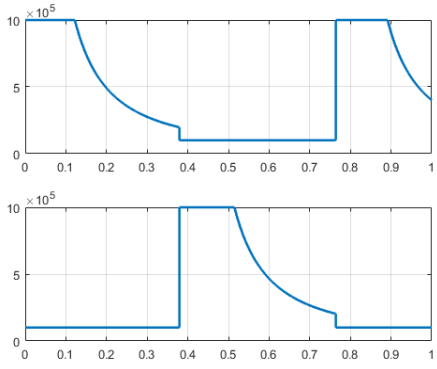

Fig. 20 Pressures in both chambers (a: upper curve, and b: lower curve) X: Time [s], Y: Pressure [bar]

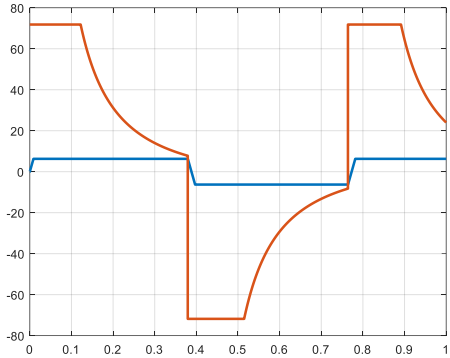

Fig. 21 Torque applied to the rotor (red) and rotor speed (blue). X: Time [s], Y: Torque [Nm], speed [rad/s]

From the pressures in the chambers and the surface of the wing, the force acting on both sides of the wing are calculated, as well as the generated torque, considering the radius of the force's action. The torque produced through the pressure in the chambers is represented in Fig. 21 (red curve). This torque produces the motion of the rotor shown by the blue curve in the figure. This curve corresponds to the speed of the rotor which is limited in both directions through the motion rectifier which drives the generator at a constant speed of 6.28 rad/s.

Between the clockwise and the anti-clockwise motions, the rotor undergoes a speed-reversal. During the reversal, the roller-clutches of the free-wheeling devices in the motion rectifier are inactive, and no torque is transmitted to the output shaft. This can be observed on the curve of Fig. 22, where the torque effectively transmitted to the output of the rectifier is shown. By the change from a positive to a negative value of the speed, one can see a zero segment of the duration of the speed reversal. Finally, the mechanical power at the output of the rectifier can be represented (Fig. 23). The instantaneous value of the power (blue curve) corresponds to the value of the transmitted torque multiplied by the value of the rotational speed. In the figure, the average value of the power is also represented.

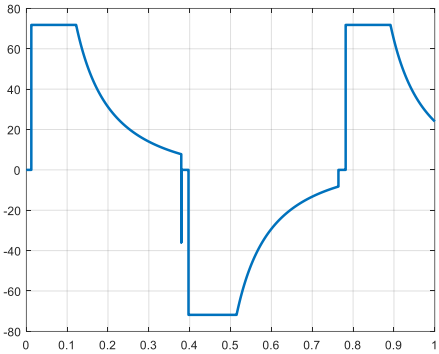

Fig. 22 Torque transmitted to the output of the motion rectifier [Nm]

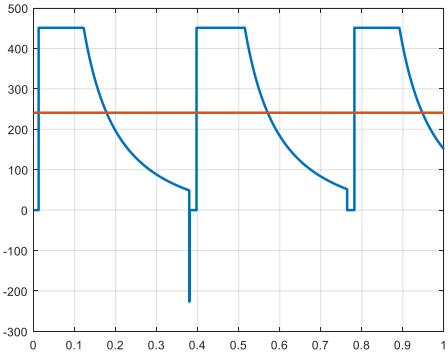

Fig. 23 Mechanical power and average at the output of the motion rectifier [W]

5. Experimental Set-Up

The different systems with enhanced efficiency have been realized as prototypes for demonstration. Fig. 24 shows the complete system with two cascaded actuators. In the middle of the figure, the motion rectifier can be shown. Left in the figure, the electric generator, and right, the coupled actuators with the intake, transfer and exhaust valves.

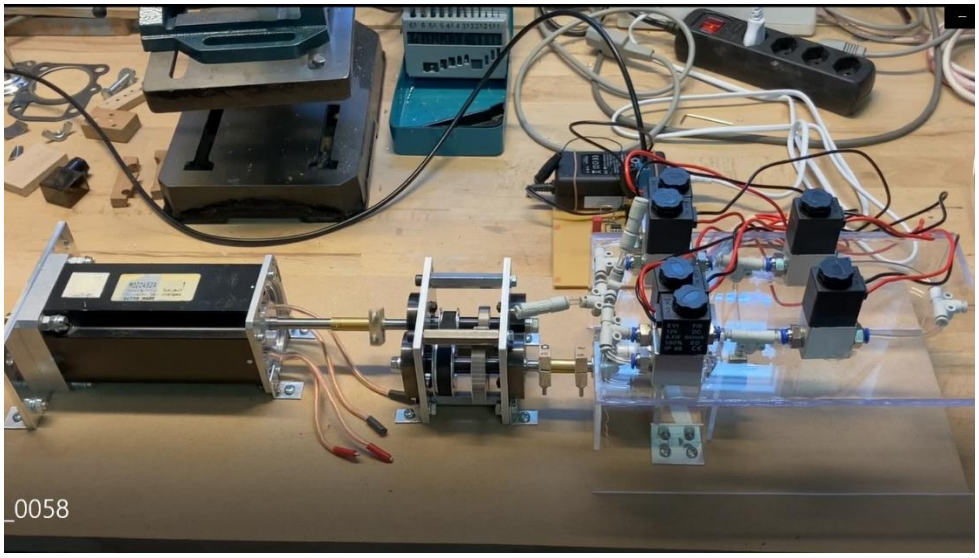

Fig. 24 Experimental set-up of the two coupled actuators

The used actuators are of the type CRB2 BW30 (11.3cm^3) and CRB2 BW20 (4.8 cm^3).

In Figure 25, the motion rectifier can be seen with its direct and inverting trains. In Fig. 26, the two coupled actuators are represented.

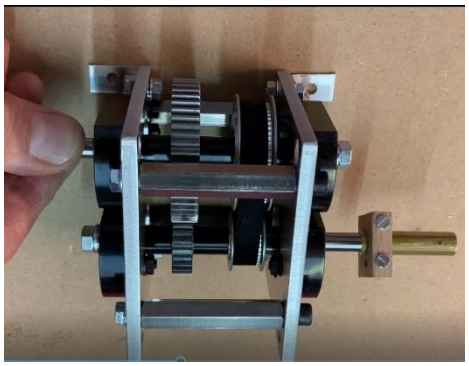

Fig. 25 The motion rectifier

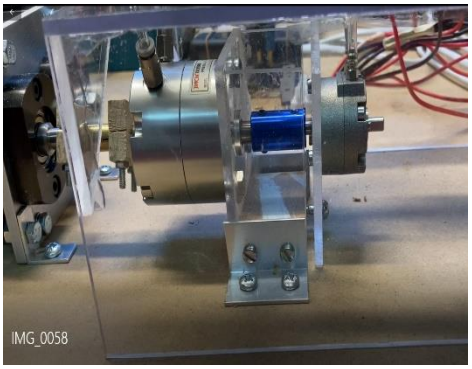

Fig. 26 The two coupled actuators

Finally, Fig. 27 shows the system with one actuator only where the displacement and expansion work are produced. Between the motion rectifier (middle of the figure) and the single actuator, the position sensors can be observed.

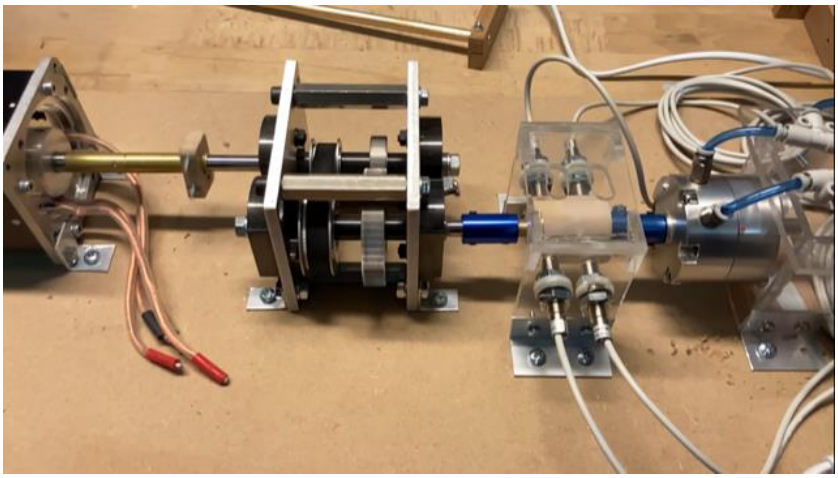

Fig. 27 The system with one actuator only

Figure 28 shows the evolution of the pressure in the two chambers of the single actuator with integrated expansion according to the scheme of Fig. 14. These curves correspond to the theoretical curves which were simulated (Fig. 20) but show some differences mainly due to the limited performances of valves and tubing. The different phases are indicated: Intake, expand and exhaust.

For the intake phase, the pressure in the chambers does not establish instantaneously, but rises according to an exponential form, mainly caused by the small section of the tubes and of the valves. Then, the expansion phase lasts over a reduced time and a reduced expansion ratio. This is due to delays of the control valves as can be shown in Fig 29. The period of one cycle is 150ms

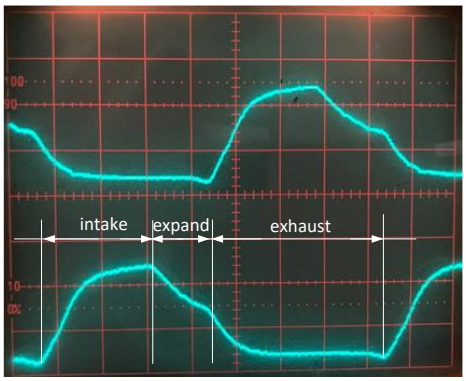

Fig. 28 Pressures in the chambers a: upper curve b: lower curve

The left picture of Fig. 29 shows the relation between the sensor signal “End of stroke” of the chamber b and the pressure in the chamber a. Before the sensor signal rises, the chamber a is in its exhaust phase. The pressure is not at the level of the atmospheric pressure but takes the value of a pressure difference ΔP_{exh} caused by the exhaust flow of the air through the small valve and tubing. After the delay time ΔT_{int} the intake valve is opened.

Due to this delay, the rotor of the actuator hits its end of stroke stop after ΔT_{mech} instead of being braked pneumatically by the opening of the intake valve of the chamber a. While the rotor is blocked at its stop, the exhaust flow goes to zero and the pressure decreases from ΔP_{exh} to the atmospheric level. Then, after ΔT_{int} the intake valve a opens and the pressure rises during the new intake phase.

In the right picture of Fig. 29, the relation between the sensor signal giving the length of the intake and the pressure in the corresponding chamber is represented. The sensor signal rises at a “length angle” which is the symmetric one before the end of stroke position. The signal X_int_a for real length of the intake for the corresponding chamber is activated through the SR flip flop as represented in Fig.14 (logic “and” function).

A time delay ΔT_{exp} appears between the falling edge of the sensor signal and the real beginning of the expansion. This is due to the slow response of the valve especially by closing. The delayed expansion causes a reduction of the expansion factor.

These records illustrate the limits of the realized demonstrator and the need of using fast control valves for such an application [11]. Additionally, the section of the valves and of the pipes must be chosen as large as possible, allowing fast filling and exhaust of the chambers of the actuator.

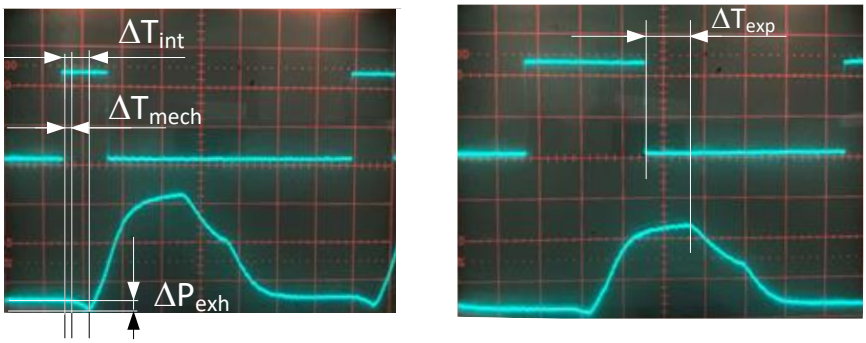

Fig. 29 Control signals and pressure in the chamber
Left/upper curve: End of stroke signal from the sensor
Left/lower curve: Pressure in the corresponding chamber
Right/upper curve: Sensor signal for the length of the intake
Right/lower curve: Pressure in the corresponding chamber

6. CONCLUSIONS

A special pneumatic drive system has been analyzed, where the energetic efficiency can be enhanced. The basic drive system using semi-rotary vane-type actuators is simulated and its energetic performance is evaluated. In this system, the alternating movement of the actuator is transmitted to an electric generator via a dedicated motion rectifier.

A first version of the drive with enhanced efficiency is proposed, where a second actuator of larger size is added with the goal to increase the mechanical performance. This system is based on the principle of extracting, in addition to the classical displacement work an additional amount of mechanical work in the form of an expansion work of the pressurized air.

A second version of the enhanced drive uses one oversized actuator only in which both the displacement work and the expansion work are realized in the same device. The principle uses two intake valves and two exhaust valves, controlled by a more complex electronic circuit and sensor system.

The three systems are simulated with an idealized model of the air transfer into the chambers. The simulation of the produced torque and mechanical work shows that the energetic performance of such a drive system can be theoretically doubled. The performances of the three systems are compared, and a corresponding efficiency is evaluated in the sense of the calculation of the produced work for an identical air consumption.

The real behavior of the systems has been tested on a small-scale experimental setup. In these real systems, the different phases of the pneumatic to mechanical transformation are well recognized through pressure measurements. The real behavior show that the dynamic phenomena related to the air transfer play a major role. Section of the tubes and of the valves as the length of the pneumatic connections must be designed specifically.

Additionally, the dynamic response of the electromagnetic valves was also observed with its impact on the system behavior and performance.

REFERENCES

[1] A. Rufer, *Energy Storage – Systems and Components*, CRC Press Taylor & Francis Group, Boca Raton FL33487-2742, ISBN-13: 978-1-138-08262-5.

[2] S. Lemofouet, Investigation and optimisation of hybrid electricity storage systems based on compressed air and supercapacitors, Thesis EPFL, 2006.

[3] M. Heidari, A. Rufer, "Fluid Flow Analysis of a New Finned Piston Reciprocating Compressor Using Pneumatic Analogy", *International Journal of Materials, Mechanics and Manufacturing*, 2014.

[4] A. Iglesias, D. Favrat, "Innovative isothermal oil-free co-rotating scroll compressor-expander for energy storage with first expander tests", *Energy Conversion and Management, Elsevier*, vol. 85, pp. 565–572, September 2014.

[5] Vane type rotary actuators, SMC Company, Series CRB2/ CRB1, CAT ES20-159 A.

[6] Z. Li, L. Zuo, J. Kuang and G. Luhrs, "Energy Harvesting shock absorber with a mechanical motion rectifier," *Smart Materials and Structures*, vol. 22, no. 025008, pp. 1–10, 2013.

[7] Dr. Mohamed Moshrefi-Torbati, *Mechanical Motion Rectifier Supervisor: Investigating the potential of a mechanical device for transforming bi-directional rotational motion into unidirectional rotational motion*. Individual Project Work Undertaken By Geoffrey Moore, Academic Year 2015/2016

[8] G. Gianfranco, Underwater electric torch with incorporated electric generator, European Patent Application EP 1 249 659 A2, 28.03.2002

[9] A. Rufer, *A compressed air driven generator with enhanced energetic efficiency* IEMERA 2020 At: Imperial College London (Virtual).

[10] M. Dagdelen, M. Sarigecili, "Friction Torque Estimation Of Vane Type Semi-Rotary Pneumatic Actuators In The Form Of Combined Coulomb-Viscous Model", In Proceedings of the 5th International Conference on Advances In Mechanical Engineering, December 2019,

[11] Festo website: Fast switching valve MHE2, Available on Web site: http://www.festo.com.

[12] S. Čajetinac, D. Šešlija, V. Nikolić, M, Todorović, "Comparison of PWM control of pneumatic actuator based on energy efficiency", *Facta Universitatis, Series: Electronics and Energetics*, vol. 25, no. 2, pp. 93–101, August 2012.